TUM/T39-95-9

December 1995

Next-To-Leading Order Analysis of Polarized and Unpolarized Structure Functions*

T.Weigl[a] and W.Melnitchouk[a,b]

[a] *Physik Department, Technische Universität München, D-85747 Garching, Germany.*

[b] *Department of Physics, University of Maryland, College Park, MD 20742, USA.*

Abstract

We present numerical solutions of the Q^2 evolution equations at next-to-leading order (NLO) for unpolarized and polarized parton distributions, in both the flavor non-singlet and singlet channels. The numerical method is based on a contour integration algorithm in complex-moment space, and, unlike most standard fitting techniques, is not restricted to the use of analytic moments of distributions. We also compute analytic continuations of the recently calculated singlet anomalous dimensions, needed for evolving polarized quark and gluon distributions at NLO. Using these we study the NLO effects on the x dependence of the spin-dependent structure functions g_1^p and g_1^n.

PACS numbers: 13.60.Hb, 13.88.+e, 14.20.Dh

Submitted to *Nuclear Physics B*.

*Work supported in part by BMBF and by DFG grant We 655/11-2

I. INTRODUCTION

One of the original testing grounds for QCD has been the study of scaling violations in structure functions in nucleon deep-inelastic scattering (DIS). Over the last 25 years a wealth of information has been accumulated on the unpolarized structure functions, $F_{1,2}$, covering some three orders of magnitude of the momentum transfer squared, Q^2, and probing the small Bjorken-x region down to $x = Q^2/2M\nu \sim 10^{-4}$, where ν is the energy transfer to the nucleon at rest, and M the nucleon mass. The data at large Q^2 ($Q^2 \gtrsim 5$ GeV^2) show no deviation from the perturbative QCD (pQCD) predictions obtained from solutions of the Dokshitzer-Gribov-Lipatov-Altarelli-Parisi (DGLAP) evolution equations [1,2]. More recently, accurate data [3,4] have also been accumulating on the spin-dependent structure functions, $g_{1,2}$, the Q^2 dependence of which will be necessary to confront the pQCD expectations.

The need for an accurate description of the Q^2 dependence of both unpolarized and polarized nucleon structure functions is severalfold. Firstly, in modeling hard processes other than DIS, the ingredients needed to calculate cross sections and event rates are parton distribution functions at a certain scale Q^2. Because the energies involved in purely hadronic reactions are often considerably larger than in DIS experiments, it is imperative that evolution of the distributions (which are extracted primarily from DIS data) to the higher Q^2 be as reliable as possible.

At the other end of the energy spectrum, describing the Q^2 behavior of structure functions at low Q^2 is no less important. While the Q^2 dependence of parton distributions is accessible to pQCD, their x dependence is of course not directly calculable. Often one tries to connect the non-perturbative content of parton distributions to valence quark models of QCD [5], which are presumed to be good approximations at $Q^2 \lesssim 1$GeV^2 (for a recent summary see Ref. [6] and references therein). To compare with data one usually evolves the leading twist component to the higher Q^2 of the DIS experiments. However, because this procedure involves evolution through a region where the strong running coupling constant, α_s, is no

longer small, one should at least take next-to-leading order (NLO) corrections into account before seriously testing the reliability of these calculations.

In the spin-dependent sector, while the kinematics in experiments involving polarization are more limited than in unpolarized processes (average Q^2 values in recent g_1 measurements only vary between 2 and 10 GeV^2), knowledge of the Q^2 dependence of polarized structure functions is essential in connection with questions concerning the spin content of the nucleon. Aside from accurately correcting for the scale dependence of first moments of polarized distributions [7], such as in the Bjorken sum rule, one also needs to understand the effects of Q^2 evolution upon the *shape* of the proton, and in particular neutron, g_1 structure functions themselves [8]. While the leading order pQCD corrections to g_1 have been known for some time, the NLO effects have until now only been calculated for non-singlet (NS) distributions. Results recently published by Mertig and van Neerven [9] for the anomalous dimensions of singlet operators at NLO have finally made it possible to compute the NLO corrections to the polarized singlet quark and gluon distributions as well.

In this paper we analyze the effects of NLO corrections on polarized and unpolarized parton distributions, in both the flavor singlet and non-singlet channels, as a function of x and Q^2. In particular, we concentrate on the Q^2 evolution of the nucleon g_1 structure function, and its effect on the x dependence at small and intermediate x. To study the effects numerically, we develop an accurate Q^2 evolution algorithm based on an inverse Mellin transform method.

Often one encounters the need to evolve distributions whose moments are not able to be expressed in simple analytic forms such as those used in standard data fitting in Refs. [10–12]. For example, most studies of structure functions in low-energy models of the nucleon, including recent attempts [13] to describe the nucleon's non-perturbative sea within the pion-cloud model [14], can only be expressed numerically, with the output needing to be parametrized before the standard evolution and fitting techniques can be applied. To facilitate evolution of both parametrized and calculated distributions, our method therefore provides for the possibility of evolving input distributions given only at a limited number of

points in Bjorken x.

The paper is organized as follows. In Section II we review the essential features of the DGLAP evolution equations at $\mathcal{O}(\alpha_s^2)$, summarizing for convenience the relevant formulas for evolution of parton distributions and structure functions. More comprehensive discussions can be found for example in Refs. [15–17]. A detailed description of the numerical method employed to perform the evolution is given in Section III. The numerical results, for both unpolarized and polarized DIS, are presented in Section IV, and conclusions are drawn in Section V. Finally, in the Appendices we collect all the relevant formulas for the LO and NLO anomalous dimensions, together with details about their extrapolation into complex moment space.

II. EVOLUTION EQUATIONS AT NEXT-TO-LEADING ORDER

In this Section we review the main features pertinent to the DGLAP evolution equations, including $\mathcal{O}(\alpha_s^2)$ corrections. We begin with the usual forward Compton amplitude, $T_{\mu\nu}$, for the scattering of a virtual photon from a nucleon,

$$T_{\mu\nu} = \frac{i}{2M} \int d^4z \; e^{iq\cdot z} \langle p, S \,|T\left(J_\mu(z) J_\nu(0)\right)| \, p, S\rangle, \tag{1}$$

where p and q are the nucleon and virtual photon four-momenta, and S is the nucleon spin vector. The fact that in the Bjorken limit ($p\cdot q, -q^2 \to \infty$) the amplitude $T_{\mu\nu}$ is light-cone dominated allows for an operator product expansion (OPE) analysis of the time-ordered product $T\left(J_\mu(z) J_\nu(0)\right)$, through which the long and short distance physics are formally separated. The singular bilocal operator $T\left(J_\mu(z) J_\nu(0)\right)$ is expanded in a basis of regular local operators, with the light-cone singularity contained in the Wilson expansion coefficient functions [18–20].

The forward Compton amplitude $T_{\mu\nu}$ is related to the nucleon DIS hadronic tensor $W_{\mu\nu}$ through the optical theorem:

$$W_{\mu\nu} = \frac{1}{\pi} \Im m T_{\mu\nu}. \tag{2}$$

The hadronic tensor is usually written in terms of the spin-independent F_1 and F_2, and spin-dependent g_1 and g_2 structure functions as:

$$W_{\mu\nu} = \frac{F_1(x,Q^2)}{M}\left(\frac{q_\mu q_\nu}{q^2} - g_{\mu\nu}\right) + \frac{F_2(x,Q^2)}{Mp\cdot q}\left(p_\mu - \frac{p\cdot q}{q^2}q_\mu\right)\left(p_\nu - \frac{p\cdot q}{q^2}q_\nu\right) + i\epsilon_{\mu\nu\alpha\beta}q^\alpha\left(\frac{S^\beta}{p\cdot q}\left(g_1(x,Q^2)+g_2(x,Q^2)\right) - p^\beta\frac{S\cdot q}{(p\cdot q)^2}g_2(x,Q^2)\right), \tag{3}$$

where $x = Q^2/2p\cdot q$ and $Q^2 = -q^2$. The structure functions are related to parton distribution functions (light-cone momentum distributions) by convoluting the latter with the Wilson coefficient functions [19,21,22], describing the hard (perturbatively calculable) photon–parton interaction. For the proton's F_2 structure function, for instance, one has:

$$F_2^p(x,Q^2) = \frac{1}{6}\int_x^1 \frac{dy}{y}\left(C_2^{NS}\left(x,Q^2\right)\ xq^{NS}\left(\frac{x}{y},Q^2\right) + \frac{5}{3}C_2^q\left(x,Q^2\right)\ x\Sigma\left(\frac{x}{y},Q^2\right) + \frac{5}{3}C_2^G\left(x,Q^2\right)\ xG\left(\frac{x}{y},Q^2\right)\right), \tag{4}$$

where $q^{NS}(x,Q^2) = (u+\bar{u}-d-\bar{d}-s-\bar{s})(x,Q^2)$ is the flavor non-singlet combination (for three flavors), while the singlet component is $\Sigma(x,Q^2) = \sum_q (q+\bar{q})(x,Q^2)$, and $G(x,Q^2)$ is the gluon distribution.

Similarly for polarized DIS, one has for the g_1 structure function of the proton:

$$g_1^p(x,Q^2) = \int_x^1 \frac{dy}{y}\left(\Delta C^{NS}(x,Q^2)\left[\frac{1}{12}\Delta q_3\left(\frac{x}{y},Q^2\right) + \frac{1}{36}\Delta q_8\left(\frac{x}{y},Q^2\right)\right] + \frac{1}{9}\Delta C^q\left(x,Q^2\right)\ \Delta\Sigma\left(\frac{x}{y},Q^2\right) + \frac{1}{9}\Delta C^G\left(x,Q^2\right)\ \Delta G\left(\frac{x}{y},Q^2\right)\right), \tag{5}$$

where the polarized singlet distribution is $\Delta\Sigma(x,Q^2) = \sum_q(\Delta q + \Delta\bar{q})(x,Q^2)$, $\Delta G(x,Q^2)$ is the polarized gluon distribution, and the non-singlet combinations Δq_3 and Δq_8 are (for three flavors) given by:

$$\Delta q_3(x,Q^2) = \left(\Delta u + \Delta\overline{u} - \Delta d - \Delta\overline{d}\right)(x,Q^2), \tag{6a}$$

$$\Delta q_8(x,Q^2) = \left(\Delta u + \Delta\overline{u} + \Delta d + \Delta\overline{d} - 2\left(\Delta s + \Delta\overline{s}\right)\right)(x,Q^2). \tag{6b}$$

Note that the polarized quark singlet coefficient function $\Delta C^q(x,Q^2) = \delta(1-x) + \mathcal{O}(\alpha_s)$, while the polarized gluon enters only at NLO, $\Delta C^G(x,Q^2) = \mathcal{O}(\alpha_s)$. We shall return to this point in Section IV B.

A. Evolution of Parton Distributions

The Q^2 evolution of parton distribution functions is most naturally expressed in terms of their moments, by solving the renormalization group equations. Defining the nth Mellin moment of a parton distribution $q(x,Q^2)$ by:

$$\mathcal{Q}_n(Q^2) = \int_0^1 dx\ x^{n-1} q(x,Q^2), \tag{7}$$

one obtains for the NS moments:

$$\mathcal{Q}_n^{NS}(Q^2) = \left[1 + \frac{\alpha_s(Q^2)-\alpha_s(\mu^2)}{4\pi}\left(\frac{\gamma_{NS}^{(1),n}}{2\beta_0} - \frac{\beta_1\gamma_{NS}^{(0),n}}{2\beta_0^2}\right)\right]\left(\frac{\alpha_s(Q^2)}{\alpha_s(\mu^2)}\right)^{\gamma_{NS}^{(0),n}/2\beta_0}\mathcal{Q}_n^{NS}(\mu^2), \tag{8}$$

where $\gamma_{NS}^{(0,1),n}$ are the anomalous dimensions at leading and next-to-leading orders, and μ^2 is some reference scale. The constants β_0, β_1 are the expansion coefficients of the Gell-Mann–Low function $\beta(Q^2)$ up to next-to-leading order:

$$\beta_0 = 11 - \frac{2}{3}N_f, \qquad \beta_1 = 102 - \frac{38}{3}N_f, \tag{9}$$

for N_f active quark flavors. Note that Eq.(8) is expressed within the $\overline{\rm MS}$ factorization scheme — for the connection to other factorization schemes see Appendix B.

Because of mixing between local operators of the OPE which are singlets under SU(N_f) transformations, one has coupled evolution equations for the singlet parton densities:

$$\begin{aligned}\begin{pmatrix}\Sigma_n(Q^2)\\ \mathcal{G}_n(Q^2)\end{pmatrix} = \Bigg\{&\left(\frac{\alpha_s(Q^2)}{\alpha_s(\mu^2)}\right)^{\lambda_-^n/2\beta_0}\Bigg[\mathbf{P}_-^n - \frac{1}{2\beta_0}\frac{\alpha_s(\mu^2)-\alpha_s(Q^2)}{4\pi}\mathbf{P}_-^n\mathbf{R}^n\mathbf{P}_-^n\\ &-\left(\frac{\alpha_s(\mu^2)}{4\pi} - \frac{\alpha_s(Q^2)}{4\pi}\left(\frac{\alpha_s(Q^2)}{\alpha_s(\mu^2)}\right)^{(\lambda_+^n-\lambda_-^n)/2\beta_0}\right)\frac{\mathbf{P}_-^n\mathbf{R}^n\mathbf{P}_+^n}{2\beta_0+\lambda_+^n-\lambda_-^n}\Bigg]\\ &+(+\longleftrightarrow -)\Bigg\}\begin{pmatrix}\Sigma_n(\mu^2)\\ \mathcal{G}_n(\mu^2)\end{pmatrix},\end{aligned} \tag{10}$$

where $\mathbf{R}^n, \mathbf{P}_\pm^n$ and $\lambda_\pm$ are given by:

$$\mathbf{R}^n = \boldsymbol{\gamma}^{(1),n} - \frac{\beta_1}{\beta_0}\boldsymbol{\gamma}^{(0),n}, \tag{11a}$$

$$\mathbf{P}^n_\pm = \pm \frac{\boldsymbol{\gamma}^{(0),n} - \lambda^n_\mp}{\lambda^n_+ - \lambda^n_-}, \tag{11b}$$

$$\lambda^n_\pm = \frac{1}{2}\left(\gamma^{(0),n}_{qq} + \gamma^{(0),n}_{GG} \pm \sqrt{(\gamma^{(0),n}_{GG} - \gamma^{(0),n}_{qq})^2 + 4\gamma^{(0),n}_{qG}\gamma^{(0),n}_{Gq}}\right), \tag{11c}$$

$$\boldsymbol{\gamma}^{(k),n} = \begin{pmatrix} \gamma^{(k),n}_{qq} & \gamma^{(k),n}_{qG} \\ \\ \gamma^{(k),n}_{Gq} & \gamma^{(k),n}_{GG} \end{pmatrix}, \quad k = 0, 1. \tag{11d}$$

For polarized parton distributions one has identical evolution equations to those in Eqs.(8) and (10), with $\mathcal{Q}_n, \Sigma_n, \mathcal{G}_n$ replaced by their spin-dependent counterparts $\Delta\mathcal{Q}_n, \Delta\Sigma_n, \Delta\mathcal{G}_n$. The differences in the evolution arise from the anomalous dimensions, which are in general different for polarized and unpolarized processes. The explicit expressions for these at LO and NLO are given in Appendix A.

The anomalous dimensions are also related to the Mellin moments of the splitting functions $P_{ij}(z)$ $(i, j = q, G)$:

$$\gamma^n_{ij} \sim \int_0^1 dz\ z^{n-1}\ P_{ij}(z), \tag{12}$$

where $P_{ij}(z)$ gives the light-cone probability of finding a parton i inside parton j, carrying a fraction z of the parent parton's light-cone momentum. If the splitting functions (or the anomalous dimensions) are known, then once the input parton distribution is fixed at a scale μ^2, the Q^2 dependence of its moments can be calculated via Eqs.(8) and (10). The x-dependent distribution at the new scale Q^2 is then obtained by inverting the Mellin transform in Eq.(7).

B. Evolution of Structure Functions

From the evolved parton distributions one can obtain the measured structure functions in two ways. Firstly, one can evolve the parton distributions, then convolute the result with the corresponding Wilson coefficient functions, as in Eqs.(4) and (5). In practice, however, to accurately determine the convolution integral requires interpolating the evolved

distribution, thereby introducing an additional source of numerical error. Alternatively, the evolved moments can be multiplied by the corresponding moments of the Wilson coefficient functions, before reconstructing the structure function via the inverse Mellin transform. In this work we adopt this second method to evaluate the structure function evolution.

The explicit relations between the moments of the non-singlet and singlet parts of the F_2 structure function and the corresponding moments of the parton distributions are:

$$\mathcal{F}_{2,n}^{NS}(Q^2) = C_{2,n}^{q}(Q^2)\ \mathcal{Q}_n^{NS}(Q^2), \tag{13}$$

$$\mathcal{F}_{2,n}^{S}(Q^2) = C_{2,n}^{q}(Q^2)\ \Sigma_n(Q^2)\ +\ C_{2,n}^{G}(Q^2)\ \mathcal{G}_n(Q^2). \tag{14}$$

For the F_3 structure function, in the case of neutrino–nucleon scattering, one has:

$$\mathcal{F}_{3,n}(Q^2) = C_{3,n}^{q}(Q^2)\ \mathcal{Q}_n^{V}(Q^2), \tag{15}$$

where $\mathcal{Q}_n^V(Q^2)$ represents the nth moment of the total valence distribution. Up to NLO in the $\overline{\rm MS}$ scheme the Wilson coefficients are given by:

$$C_{k,n}^{NS}(Q^2) = C_{k,n}^{q}(Q^2) = C_{k,n}^{(0),q} + \frac{\alpha_s(Q^2)}{4\pi} C_{k,n}^{(1),q}, \tag{16}$$

$$C_{k,n}^{G}(Q^2) = C_{k,n}^{(0),G} + \frac{\alpha_s(Q^2)}{4\pi} C_{k,n}^{(1),G}, \qquad k = 2, 3, \tag{17}$$

where

$$C_{2,n}^{(0),q} = 1, \tag{18a}$$

$$C_{2,n}^{(1),q} = C_F \left[2S_1^2(n) - 2S_2(n) + 3S_1(n) - \frac{2S_1(n)}{n(n+1)} + \frac{3}{n} + \frac{4}{n+1} + \frac{2}{n^2} - 9 \right], \tag{18b}$$

$$C_{3,n}^{(0),q} = 1, \tag{18c}$$

$$C_{3,n}^{(1),q} = C_F \left[2S_1^2(n) - 2S_2(n) + 3S_1(n) - \frac{2S_1(n)}{n(n+1)} + \frac{1}{n} + \frac{2}{n+1} + \frac{2}{n^2} - 9 \right], \tag{18d}$$

$$C_{2,n}^{(0),G} = 0, \tag{18e}$$

$$C_{2,n}^{(1),G} = -4T_F \left[S_1(n) \frac{n^2+n+2}{n(n+1)(n+2)} + \frac{1}{n} - \frac{1}{n^2} - \frac{6}{n+1} + \frac{6}{n+2} \right], \tag{18f}$$

with $C_F = 4/3$ and $T_F = N_f/2$. The functions S_1 and S_2 are given in Appendix A 1.

The analogous expression for the moments of the polarized structure function $g_1(x, Q^2)$ (for $N_f = 3$) is:

$$\mathcal{G}_{1,n}(Q^2) = \Delta C_n^{NS}(Q^2) \left(\pm \frac{1}{12} \Delta q_{3,n}(Q^2) + \frac{1}{36} \Delta q_{8,n}(Q^2) \right) + \frac{1}{9} \Delta C_n^q(Q^2) \Delta \Sigma_n(Q^2) + \frac{1}{9} \Delta C_n^G(Q^2) \Delta G_n(Q^2), \tag{19}$$

where $\pm$ refers to the proton and neutron, respectively. The polarized Wilson coefficients ΔC_n are given by [9,23]:

$$\Delta C_n^{NS}(Q^2) = \Delta C_n^q(Q^2) = \Delta C_n^{(0),q} + \frac{\alpha_s(Q^2)}{4\pi} \Delta C_n^{(1),q}, \tag{20}$$

$$\Delta C_n^G(Q^2) = \Delta C_n^{(0),G} + \frac{\alpha_s(Q^2)}{4\pi} \Delta C_n^{(1),G}, \tag{21}$$

where

$$\Delta C_n^{(0),q} = 1, \tag{22a}$$

$$\Delta C_n^{(1),q} = C_F \left[2S_1^2(n) - 2S_2(n) + \frac{2S_1(n)}{n+1} - \frac{2S_1(n)}{n} + 3S_1(n) - \frac{2}{n(n+1)} + \frac{3}{n} + \frac{2}{n^2} - 9 \right], \tag{22b}$$

$$\Delta C_n^{(0),G} = 0, \tag{22c}$$

$$\Delta C_n^{(1),G} = T_F \left[\frac{4(n-1)(1-n-nS_1(n))}{n^2(n+1)} \right]. \tag{22d}$$

As in the unpolarized case, one has to use anomalous dimensions and Wilson coefficients calculated consistently within the same factorization scheme. For the NLO evolution of both unpolarized and polarized distributions we work within the $\overline{\text{MS}}$-scheme throughout. A property of this scheme is that $\Delta C_{n=1}^G = 0$, resulting in zero gluonic contribution to the first moment of g_1, and hence no correction to the Ellis-Jaffe sum rule [24]. All other moments of the structure function $g_1(x, Q^2)$ do, however, contain gluonic corrections.

III. NUMERICAL SOLUTION

Having outlined the essential features of the DGLAP evolution equations, we next examine methods which can be used to efficiently and reliably extract their solutions. The

most direct approach involves simply integrating the integro-differential version of the equations directly (see e.g. Ref. [25]). With this method, to obtain evolved distributions in the range $[x_0, 1]$ the input distribution needs to be known only for $x > x_0$. However, many iterations are necessary to obtain accurate results when evolving over a large range of Q^2, which consequently decreases both the efficiency and accuracy of the evolution. Other proposed methods have made use of complete sets of orthogonal polynomials, such as Bernstein polynomials [26] or Laguerre polynomials [27]. Difficulties exist, however, in applying these methods to regions of very small or very large x. Instead, we will follow an approach using the Mellin transform technique [28], similar to that discussed in Ref. [12], but differing in a number of aspects which we now discuss.

A. Contour Method

The advantage of the Mellin transform (or contour integration) technique lies in its simplicity, and efficiency with computing time. In the past this method has been applied in cases where the moments of the input distributions were known in analytic form, such as when $q(x)$ is a linear combination of terms of the form $ax^b(1-x)^c$ or similar [12]. The need often exists, however, to evolve input distributions which are not able to be expressed in this form. For example, one may wish to evolve distributions obtained from model calculations [6], which generally do not have a simple analytic form. Therefore it is necessary that one has available an accurate NLO evolution procedure for applications where the input distributions are known only at a limited number of points in x.

The main steps involved in the Mellin transform technique can be summarized as follows:

- The Mellin moments of the input distributions $\mathcal{Q}_n(\mu^2)$ are calculated numerically at the input scale μ^2.
- The calculated moments are evolved to the scale Q^2 via Eqs.(8)and (10).
- The parton distributions are reconstructed via the inverse Mellin transformation:

$$q(x,Q^2) = \frac{1}{2\pi i}\int_{c-i\infty}^{c+i\infty} dn\ x^{-n}\mathcal{Q}_n(Q^2). \tag{23a}$$

In practice it is more convenient to express Eq.(23a) as an inverse Laplace transformation:

$$q(x,Q^2) = \frac{1}{2\pi i}\int_{c-i\infty}^{c+i\infty} dn\ e^{n(-\ln x)}\ \mathcal{Q}_n(Q^2). \tag{23b}$$

One disadvantage in principle of this method is that in order to calculate the moments of distributions, the input must be known in the entire x-region $[0,1]$. However, as will be seen in Section IV, the restriction to the interval $[x_0,1]$ has negligible effects numerically.

B. Evaluation of Moments

If the input distribution is of the form $q(x,\mu^2) = ax^b(1-x)^c$, its moments are simply expressed in terms of Beta functions B:

$$\mathcal{Q}_n = aB(n+b,c+1) = a\frac{\Gamma(n+b)\Gamma(c+1)}{\Gamma(n+b+c+1)}. \tag{24}$$

If the analytic moments are not available, each Mellin moment must be integrated numerically. This causes difficulties, however, for complex values of n, since the integrand in Eq.(23b) oscillates rapidly as $x \to 0$. This can be seen by writing $n = c + id$, where c, d are real:

$$\mathcal{Q}_n(\mu^2) = \int_0^1 dx\ x^{-1+c}e^{id\ln x}\ q(x,\mu^2). \tag{25a}$$

In practice it is easier to perform the integration by making the substitution $\ln x \to t$, which gives an integrand that oscillates with constant frequency:

$$\mathcal{Q}_n(\mu^2) = \int_{-\infty}^0 dt\ e^{(c-1)t}e^{idt}q(e^t,\mu^2). \tag{25b}$$

The real and imaginary parts of this integral are then evaluated separately by using a suitable adaptive quadrature algorithm (such as that provided by the IMSL numerical library routine

DQDAWO [29]). This way accurate moments can be obtained for any input distribution given as a function of Bjorken-x over the entire region, $0 \leq x \leq 1$.

Two additional problems arise when using input that is given only at a limited number of x-points. Firstly, without an adaptive quadrature routine the moments are often inaccurate, with the error increasing with the imaginary part of n. One is then forced to interpolate the input between the x-points, which leads to a second problem, namely that the x-range covered by these input points is limited to $x_0 \leq x \leq x_1$.

Clearly the quality of the moments, and hence the accuracy of the evolved parton distributions, depends strongly on the quality of the interpolation routine. For this we have used cubic splines and higher order B-splines, both with a 'not-a-knot' condition (see e.g. IMSL routines DCSINT and DBSINT, respectively [29]). Taking equidistant x-points leads to very good results everywhere except in the neighborhood of the boundaries at $x = x_0$ and x_1. To obtain sufficiently good results over the entire x-range one should choose the location of x-points suitably, in particular more points near the boundaries than in between.

C. Numerical Inversion

The final step, which is numerically the most difficult, is the contour integration in the inverse Mellin (or Laplace) transformation. Depending on the value of Bjorken-x at which the parton distribution is to be reconstructed, two different methods are employed for the regions $x < 0.80$ and $x \geq 0.80$.

In the $x < 0.80$ region Crump's method [30] is applied (using e.g. the IMSL routine DINLAP [29]), in which the inverse Laplace transform of the function $F(n)$ is approximated by a partial sum of a Fourier representation:

$$f(t) \simeq \frac{e^{ct}}{\tau}\left[\frac{1}{2}F(c) + \sum_{k=1}^{\infty}\left\{\Re e\left(F\left(c + k\pi i/\tau\right)\right)\cos\frac{k\pi t}{\tau} - \Im m\left(F\left(c + k\pi i/\tau\right)\right)\sin\frac{k\pi t}{\tau}\right\}\right]. \quad (26)$$

The value of c has to be on the right side of all singularities appearing in $F(n)$. From Regge physics one obtains the conditions $\Re e\ n \geq 2$ and $\Re e\ n \geq 1$ for the singlet and

non-singlet distributions, respectively. The parameter τ controls the step length in the imaginary direction. This method fails, however, when $f(t)$ reaches values close to zero, which occurs for large x. In the kinematic range $x \geq 0.8$ we therefore utilize an alternative algorithm, in which the inverse Laplace transform is computed via a Laguerre expansion (see e.g. IMSL routine DSINLP [29]). The performance of this procedure has been checked by first performing the Mellin transform by computing the moments, and then transforming back with the above routines to compare the output with the original input.

One further comment should be made about the small-x region. It is in general more problematic to compute the inverse Laplace transform $f(t)$ numerically when t is very large, or equivalently when x is very small. In practice we find that the above procedure gives reliable results for parton distributions at least down to x values reached by current experiments at HERA, namely $x \sim 10^{-4}$.

D. Computation of the Running Coupling Constant

If one performs evolution at low values of Q^2, care must be taken when calculating the running coupling constant α_s. At NLO, α_s can be computed exactly by solving the transcendental equation numerically:

$$\ln \frac{Q^2}{\Lambda^2_{QCD}} - \frac{4\pi}{\beta_0 \alpha_s} + \frac{\beta_1}{\beta_0^2} \ln \left[\frac{4\pi}{\beta_0 \alpha_s} + \frac{\beta_1}{\beta_0^2} \right] = 0, \tag{27}$$

as obtained from the renormalization group analysis. For small values of α_s one can find approximate solutions by using the formula:

$$\alpha_s(Q^2) \approx \frac{4\pi}{\beta_0 \ln Q^2/\Lambda^2_{QCD}} - \frac{4\pi\beta_1}{\beta_0^3} \frac{\ln \ln Q^2/\Lambda^2_{QCD}}{\ln^2 Q^2/\Lambda^2_{QCD}}. \tag{28}$$

In practice this approximation turns out to be accurate only for $Q^2 \gtrsim 1$ GeV^2. At smaller scales, $Q^2 \approx 0.4$ GeV^2, the error in α_s is about 7% (with $\Lambda_{QCD} = 200$ MeV in both Eq.(27) and (28) and $N_f = 3$). In the region $Q^2 \approx 0.2$ GeV^2 from which low energy model calculated input is often evolved, use of the approximation Eq.(28) can give errors of up to 20% in the

running coupling for the same values of Λ_{QCD} and N_f. The discrepancy becomes bigger still for larger Λ_{QCD}. Of course Λ_{QCD} itself can be extracted using Eq.(28) from data at large Q^2, since there the difference between Eqs.(27) and (28) is minimal, however the use of Eq.(28) outside this region could be problematic given the above differences.

IV. RESULTS

Using the numerical method described in Section III, we present here the results of the evolution of parton densities including all the NLO corrections. We should stress that our aim is not to perform a complete fit to the available data — such programs of data parametrizations are adequately addressed in Refs. [10–12], for example. Our purpose will be to simply demonstrate the potential differences in the evolved distributions when order α_s^2 corrections are taken into account. After first establishing the degree of accuracy and the region of reliability of the evolution program in the unpolarized sector, we then turn our attention to the more topical discussion of evolution of polarized distributions at NLO.

A. Unpolarized Distributions

To demonstrate the effect of the numerical algorithm on a typical parton distribution, for the spin-averaged distributions we take as input the latest parametrization from the CTEQ collaboration [11]:

$$xu_V(x) = 1.37x^{0.497}(1-x)^{3.74}(1+6.25x^{0.880}), \tag{29a}$$

$$xd_V(x) = 0.801x^{0.497}(1-x)^{4.19}(1+1.69x^{0.375}), \tag{29b}$$

$$xG(x) = 0.738x^{-0.286}(1-x)^{5.31}(1+7.30x), \tag{29c}$$

$$x(\bar{d}(x)+\bar{u}(x)) = 0.1094x^{-0.286}(1-x)^{8.34}(1+17.5x), \tag{29d}$$

given at $Q^2 = 2.56$ GeV^2. Evolution at NLO is carried out in the $\overline{\rm MS}$ scheme, using $\Lambda_{QCD} = 239$ MeV for $N_f = 4$ flavors, and taking into account the charm threshold at

Q^2 =(1.6 GeV)^2. (Although the effect of neglecting the charm threshold increases with decreasing Q^2, even when evolving down to $Q^2 \sim 0.5$ GeV^2 it is still very small.)

To illustrate the performance of the evolution algorithm, we first examine NLO evolution of the total valence distribution, $x(u_V + d_V)$. In Fig.1 the program's accuracy is illustrated when using different numbers of points, N_x, in Bjorken-x, with the input evolved to $Q^2 = 100$ GeV^2. With $N_x = 50$ points in the range [0.005,1], the results are indistinguishable from those obtained by calculating the moments of (29a,29b) analytically. In this case the effect of changing the lower limit of integration from $x_0 = 0$ to $x_0 > 0$ is negligible. Excellent results can be attained for nearly all x even with $N_x = 25$ (solid curve, marked "$i25$" in Fig.1). Decreasing the number of points to $N_x = 13$ has very little effect in the intermediate-x region, $0.2 \lesssim x \lesssim 0.8$, but at larger x the accuracy becomes somewhat worse. For comparison, we also show in Fig.1 (dashed curves) the results obtained by calculating moments via a simple histogram method,

$$\begin{aligned} \mathcal{Q}_n(Q^2) &= \int_0^1 dx\ x^{n-2} \left(xq(x,Q^2) \right) \\ &\approx \sum_{i=1}^{N_x} x_i q(x_i,Q^2) \left(\frac{x_i^{n-1} - x_{i-1}^{n-1}}{n-1} \right). \end{aligned} \tag{30}$$

For $N_x = 50$ the discrepancy with the interpolation method is rather more dramatic, particularly at large x, and to obtain a similar degree of accuracy one needs N_x in excess of 1000. Similar accuracy will also be obtained when evolving different input distributions, such as those from Refs. [6,10,12].

In Fig.2 we compare the valence $x(u_V+d_V)$ distribution evolved with leading and next-to-leading order corrections. For the LO evolution we use $\Lambda_{QCD} = 177$ MeV, according to the latest fit results from Ref. [11]. To avoid ambiguities associated with the factorization scheme dependence of the (generally unphysical) NLO distributions, we work in the DIS scheme. (Differences between distributions calculated in different schemes are of order $\alpha_s(Q^2)$ [31], and while negligible at high Q^2, they can become quite large at $Q^2 \lesssim 1$ GeV^2.) Although in general input distributions at LO and NLO need not be identical, especially when one seeks precisions fits to DIS data, we will simply demonstrate the effects by assuming the

input shapes to be the same. This assumption is an implicit one, for example, in low-energy effective model calculations of leading twist parton distributions [5,6], where because the input model scale is *a priori* unknown, the same calculated distribution must be evolved with either LO or NLO corrections.

The main effect of NLO corrections on the valence distributions (with upwards evolution) is to make them softer compared to those evolved with LO corrections only. Conversely, NLO evolution produces somewhat harder distributions when evolved downwards to low scales $Q^2 = 0.5$ GeV^2, such as those associated with valence distributions calculated from low-energy (constituent quark) models of QCD.

In connection with this, we should note that uncertainty in the precise value of Λ_{QCD} (the Particle Data Group gives 234 ± 56 MeV [32]) can be translated into quite a significant difference in the starting scale Q_0^2 for the evolution of the calculated model results. Taking the upper and lower values of $\Lambda_{QCD} = 290$ and 178 MeV, one obtains essentially identical shapes of the evolved distributions with $Q_0^2 = 1$ and 0.5 GeV^2, respectively. Even given the fact that the exact scale for such model calculations is a priori unknown, a factor 2 (!) represents quite a large effect in the phenomenology of the scale dependence of low-energy model distributions.

Turning now to the singlet sector, we illustrate in Fig.3 the effects of NLO corrections on the distribution $\Sigma(x, Q^2)$. Taking the CTEQ parametrization at $Q_0^2 = 2.56$ GeV^2 as input, the distribution is evolved to $Q^2 = 10$ and 100 GeV^2 using the DIS scheme to compare physical quantities at LO and NLO (in the DIS scheme $x\Sigma(x, Q^2)$ represents the structure function F_2 measured in deep-inelastic neutrino-nucleon scattering). The results here have been obtained with $N_x = 60$ on a logarithmic scale in Bjorken-x, and agree to within 0.01% with those using analytic moments. Similar accuracy is obtained also for the singlet gluon distribution.

Having established the quality of performance of our numerical method for both non-singlet and singlet evolution of unpolarized distributions, in the next Section we discuss the NLO effects on polarized parton densities.

B. Polarized Distributions

Evolution of polarized parton distributions in the non-singlet sector is straightforward, since at NLO it is governed by exactly the same anomalous dimensions as for unpolarized DIS. Therefore the effects are identical to those in Figs.1 and 2. In the singlet sector, on the other hand, the anomalous dimensions for polarized and unpolarized scattering are very different. In fact, due to the complexity of the problem, the relevant splitting functions and anomalous dimensions necessary to describe the NLO singlet evolution as a function of x have only recently been calculated [9]. A recalculation by Vogelsang [35], using an independent method, has confirmed the results in [9]. To use the inverse Mellin method for the evolution, it is necessary to analytically continue the results of Ref. [9] into the complex-n plane. In doing so care must be taken since, unlike for the unpolarized distributions, the continuations for spin-dependent structure functions are performed from odd moments. The full details of the continuation can be found in Appendix A 2 [1].

To illustrate the role of NLO corrections in spin-dependent distributions, we have used as input the global fit by Gehrmann and Stirling (Set A) [36]:

$$x\Delta u_V(x) = 0.327x^{0.46}(1-x)^{3.64}(1+18.36x), \tag{31a}$$

$$x\Delta d_V(x) = -0.139x^{0.46}(1-x)^{4.64}(1+18.36x), \tag{31b}$$

$$x\Delta\overline{u}(x) = x\Delta\overline{d}(x) \;=\; x\Delta\overline{s}(x) \;=\; x\Delta c(x) \;=\; 0, \tag{31c}$$

$$x\Delta G(x) = 16.64\,x\,(1-x)^{7.44}, \tag{31d}$$

with a starting scale of $Q^2 = 4$ GeV^2. Following Ref. [36], in LO we again perform the evolution with three active flavors and $\Lambda^{LO}_{QCD} = 177$ MeV, as for the unpolarized evolution

[1] While completing this paper, similar NLO analyses of polarized distributions in Refs. [33,34] came to our attention. A different prescription for continuation of the singlet polarized anomalous dimensions into complex-n space is used in Ref. [33], although we have checked that numerically these are in fact equivalent — see Appendix A 2.

above. However, contrary to the procedure adopted in [36], we omit the anomalous gluon term when calculating the structure functions $g_1^p(x,Q^2)$ and $g_1^n(x,Q^2)$ at leading order. This term arises only at NLO, and in a consistent treatment should only be included in NLO evolution — see Eqs.(5) and (19). In NLO we also use three active flavors, and a different value of $\Lambda_{QCD}^{NLO} = 239$ MeV, corresponding to that obtained by CTEQ in their fits to unpolarized parton distributions. As in the discussion of the unpolarized evolution in Sec.IV A, for illustration purposes we take the same input shape for both LO and NLO evolution.

In Fig.4 the x dependence of $\Delta\Sigma(x,Q^2)$, evolved down to 2 GeV^2 and up to 10 GeV^2, is shown between $x = 10^{-4}$ and 1. The difference between distributions evolved in LO and NLO can be sizeable below $x \approx 5 \times 10^{-3}$, and even larger with decreasing x. Furthermore, it is interesting to observe that at $Q^2 = 10$ GeV^2 even the curvature changes sign compared to the LO result. Similarly large differences between LO and NLO evolution appear for the polarized gluon distribution, $\Delta G(x,Q^2)$, at small x — see Fig.5. These dramatic effects are largely independent of the shapes of the input LO and NLO distributions, and can be traced back to the dominant role played by NLO corrections at small x. This becomes evident if one considers the $x \to 0$ behavior of the splitting functions $P_{ij}(x) = P_{ij}^{(0)}(x) + (\alpha_s/4\pi)\, P_{ij}^{(1)}(x)$ [9,37] — in LO one has:

$$P_{qq}^{(0)}(x \to 0) \to 4C_F, \tag{32a}$$

$$P_{qG}^{(0)}(x \to 0) \to -8T_F, \tag{32b}$$

$$P_{Gq}^{(0)}(x \to 0) \to 8C_F, \tag{32c}$$

$$P_{GG}^{(0)}(x \to 0) \to 16C_A, \tag{32d}$$

while at NLO:

$$P_{qq}^{(1)}(x \to 0) \to \left(8C_FC_A - 16C_FT_F - 12C_F^2\right) \ln^2 x, \tag{32e}$$

$$P_{qG}^{(1)}(x \to 0) \to -\left(16C_AT_F + 8C_FT_F\right) \ln^2 x, \tag{32f}$$

$$P_{Gq}^{(1)}(x \to 0) \to \left(16C_AC_F + 8C_F^2\right) \ln^2 x, \tag{32g}$$

$$P_{GG}^{(1)}(x \to 0) \to \Big(32C_A^2 - 16C_F T_F\Big) \ln^2 x. \tag{32h}$$

For small enough x, the NLO corrections $P_{ij}^{(1)}(x)$ can become quite large and overwhelm the $\alpha_s/4\pi$ factor. Note also that even the *sign* of $P_{qq}^{(1)}(x)$ changes compared with $P_{qq}^{(0)}(x)$ as $x \to 0$ (for $C_F = 4/3, T_F = N_f/2, C_A = 3$ and $N_f \geq 2$).

With the Q^2 evolution of the polarized quark singlet and gluon distributions known, one can now examine the effect of NLO corrections on the spin-dependent structure function $g_1(x, Q^2)$. In Fig.6 we show the proton structure function $xg_1^p(x, Q^2)$, evolved to the averaged scale $Q^2 = 10$ GeV^2 at which the SMC data [3] were taken. The important result to notice is that the NLO corrections are large in the range of x covered by the experiment. In the region $x \sim 0.2$ the corrections can in fact be of the same order of magnitude as the quoted error bars on the data. Furthermore, the fact that these are negative is consistent with the known reduction of the first moment of g_1 [7] when NLO corrections are included.

In Fig.7 we also show the polarized neutron structure function $xg_1^n(x, Q^2)$, evolved at LO and NLO down to a scale $Q^2 = 2$ GeV^2 for comparison with the SLAC E142 data [4]. Because evolution here involves a somewhat lower resolution scale, the effects of NLO corrections should be be relatively larger. Clearly, one sees that these can have a potentially significant effect on the shape of the structure function, when the data points are evolved to the same value of Q^2.

V. CONCLUSION

We have examined in detail the role of NLO corrections on the shapes of the nucleon's singlet and non-singlet parton distributions, using a Q^2 evolution algorithm based on the inverse Mellin transform in complex moment space. For a complete description of polarized and unpolarized evolution at NLO it has been necessary to extrapolate recently obtained results for the polarized singlet NLO anomalous dimensions into the complex-n plane. Of particular importance are the Q^2 corrections to the spin-dependent g_1 structure functions of the proton and neutron. We find that in the region of x and Q^2 relevant to current

and upcoming experiments, the NLO effects are not negligible, and should be included in future analyses of data. Finally, we should make a note about the Q^2 behavior of the polarization asymmetry $A_1 = g_1/F_1$, which was assumed to be independent of Q^2 in previous data analyses [3,4]. While the non-singlet parts of g_1 and F_1 evolve similarly at NLO, the evolution of the singlet components is dramatically different, as seen in Figs.3–5, especially at low x. Therefore one should be wary of the possible errors introduced into g_1 at small x if one extracts this from the A_1 data under this assumption.

ACKNOWLEDGMENTS

We thank S.Kumano, E.Reya, F.M.Steffens and A.Vogt for useful discussions and communications, and in particular W.Weise for helpful comments and a careful reading of the manuscript. We also thank A.W.Schreiber for providing the LO evolution program. This work was supported by the BMBF.

APPENDIX A: ANOMALOUS DIMENSIONS

1. Unpolarized DIS

Although the results for the full anomalous dimensions up to $\mathcal{O}(\alpha_s^2)$ can be found throughout the literature, for convenience we catalogue them here in full. In the $\overline{\rm MS}$ scheme the anomalous dimensions are given by the perturbative expansion:

$$\gamma_{NS}^n(Q^2) = \frac{\alpha_s(Q^2)}{4\pi}\gamma_{NS}^{(0),n} + \left(\frac{\alpha_s(Q^2)}{4\pi}\right)^2 \gamma_{NS}^{(1),n} + \cdots, \tag{A1a}$$

$$\boldsymbol{\gamma}^n(Q^2) = \frac{\alpha_s(Q^2)}{4\pi}\boldsymbol{\gamma}^{(0),n} + \left(\frac{\alpha_s(Q^2)}{4\pi}\right)^2 \boldsymbol{\gamma}^{(1),n} + \cdots, \tag{A1b}$$

$$\boldsymbol{\gamma}^{(k),n} = \begin{pmatrix} \gamma_{qq}^{(k),n} & \gamma_{qG}^{(k),n} \\ \\ \gamma_{Gq}^{(k),n} & \gamma_{GG}^{(k),n} \end{pmatrix}, \tag{A1c}$$

where the order α_s anomalous dimensions are [2,38]:

$$\gamma_{NS}^{(0),n} = \gamma_{qq}^{(0),n} = 2\,C_F\,\left[4S_1(n) - 3 - \frac{2}{n(n+1)}\right], \tag{A2a}$$

$$\gamma_{qG}^{(0),n} = -8\,T_F\,\frac{n^2+n+2}{n(n+1)(n+2)}, \tag{A2b}$$

$$\gamma_{Gq}^{(0),n} = -4\,C_F\,\frac{n^2+n+2}{(n-1)n(n+1)}, \tag{A2c}$$

$$\gamma_{GG}^{(0),n} = 2\,C_A\,\left[4S_1(n) - \frac{11}{3} - \frac{4}{n(n-1)} - \frac{4}{(n+1)(n+2)}\right] + \frac{8}{3}T_F, \tag{A2d}$$

with $C_F = 4/3$, $T_F = N_f/2$ and $C_A = 3$. The anomalous dimensions at $\mathcal{O}(\alpha_s^2)$ are given by [38]:

$$\begin{aligned}
\gamma_{NS}^{(1),n} = C_F^2 &\left[\frac{16S_1(n)(2n+1)}{n^2(n+1)^2} + 16\left(2S_1(n) - \frac{1}{n(n+1)}\right)(S_2(n) - S_2'(n/2))\right. \\
&+24S_2(n) + 64\tilde{S}(n) - 8S_3'(n/2) - 3 \\
&\left.-8\frac{3n^3+n^2-1}{n^3(n+1)^3} - 16\eta\frac{2n^2+2n+1}{n^3(n+1)^3}\right] \\
&+C_AC_F\left[\frac{536}{9}S_1(n) - 8\left(2S_1(n) - \frac{1}{n(n+1)}\right)(2S_2(n) - S_2'(n/2))\right. \\
&\left.-\frac{88}{3}S_2(n) - 32\tilde{S}(n) + 4S_3'(n/2) - \frac{17}{3}\right.
\end{aligned}$$

$$-\frac{4}{9}\frac{151n^4+236n^3+88n^2+3n+18}{n^3(n+1)^3}+8\eta\frac{2n^2+2n+1}{n^3(n+1)^3}\Bigg]$$
$$+C_FT_F\left[-\frac{160}{9}S_1(n)+\frac{32}{3}S_2(n)+\frac{4}{3}+\frac{16}{9}\frac{11n^2+5n-3}{n^2(n+1)^2}\right], \tag{A3a}$$

$$\gamma_{qq}^{(1),n}=\gamma_{NS}^{(1),n}(\eta=1)-16C_FT_F\frac{5n^5+32n^4+49n^3+38n^2+28n+8}{(n-1)n^3(n+1)^3(n+2)^2}, \tag{A3b}$$

$$\begin{aligned}\gamma_{qG}^{(1),n}=&-8C_AT_F\left[(-2S_1^2(n)+2S_2(n)-2S_2'(n/2))\frac{n^2+n+2}{n(n+1)(n+2)}\right.\\
&+\frac{8S_1(n)(2n+3)}{(n+1)^2(n+2)^2}+2\frac{n^9+6n^8+15n^7+25n^6+36n^5+85n^4}{(n-1)n^3(n+1)^3(n+2)^3}\\
&\left.+2\frac{128n^3+104n^2+64n+16}{(n-1)^3n^3(n+1)^3(n+2)^3}\right]\\
&-8C_FT_F\left[(2S_1^2(n)-2S_2(n)+5)\frac{n^2+n+2}{n(n+1)(n+2)}-\frac{4S_1(n)}{n^2}\right.\\
&\left.+\frac{11n^4+26n^3+15n^2+8n+4}{n^3(n+1)^3(n+2)}\right],\end{aligned} \tag{A3c}$$

$$\begin{aligned}\gamma_{Gq}^{(1),n}=&-4C_F^2\left[(-2S_1^2(n)+10S_1(n)-2S_2(n))\frac{n^2+n+2}{n-1)n(n+1)}-4\frac{S_1(n)}{(n+1)^2}\right.\\
&\left.-\frac{12n^6+30n^5+43n^4+28n^3-n^2-12n-4}{(n-1)n^3(n+1)^3}\right]\\
&-8C_AC_F\left[(S_1^2(n)+S_2(n)-S_2'(n/2))\frac{n^2+n+2}{(n-1)n(n+1)}\right.\\
&-S_1(n)\frac{17n^4+41n^2-22n-12}{3(n-1)^2n^2(n+1)}+\frac{n^3+n^2+4n+2}{n^3(n+1)^3}\\
&+\frac{109n^8+512n^7+879n^6+772n^5-104n^4}{9(n-1)^2n^3(n+1)^2(n+2)^2}\\
&\left.\frac{-954n^3-278n^2+288n+72}{9(n-1)^2n^3(n+1)^2(n+2)^2}\right]\\
&-\frac{32}{3}C_FT_F\left[\left(S_1(n)-\frac{8}{3}\right)\frac{n^2+n+2}{(n-1)n(n+1)}+\frac{1}{(n+1)^2}\right],\end{aligned} \tag{A3d}$$

$$\gamma_{GG}^{(1),n}=C_AT_F\left[-\frac{160}{9}S_1(n)+\frac{32}{3}+\frac{16}{9}\frac{38n^4+76n^3+94n^2+56n+12}{(n-1)n^2(n+1)^2(n+2)}\right]$$

$$
\begin{aligned}
&+C_F T_F \left[8+16\frac{2n^6+4n^5+n^4-10n^3-5n^2-4n-4}{(n-1)n^3(n+1)^3(n+2)}\right]\\
&+C_A^2\left[\frac{536}{9}S_1(n)+64S_1(n)\frac{2n^5+5n^4+8n^3+7n^2-2n-2}{(n-1)^2n^2(n+1)^2(n+2)^2}-\frac{64}{3}\right.\\
&+32S_2'(n/2)\frac{n^2+n+1}{(n-1)n(n+1)(n+2)}\\
&-\frac{4}{9}\frac{457n^9+2742n^8+6040n^7+6098n^6+1567n^5-2344n^4-1632n^3}{(n-1)^2n^3(n+1)^3(n+2)^3}\\
&\left.+\frac{560n^2+1488n+576}{(n-1)^2n^3(n+1)^3(n+2)^3}-16S_1(n)S_2'(n/2)+32\tilde{S}(n)-4S_3'(n/2)\right].
\end{aligned}
\tag{A3e}
$$

The expressions (A2) and (A3) are also valid for complex n if the following analytic continuations are used [12]:

$$S_1(n) = \sum_{j=1}^{n}\frac{1}{j} \to \gamma_E + \Psi(n+1), \tag{A4a}$$

$$S_2(n) = \sum_{j=1}^{n}\frac{1}{j^2} \to \zeta(2) - \Psi'(n+1), \tag{A4b}$$

$$S_3(n) = \sum_{j=1}^{n}\frac{1}{j^3} \to \zeta(3) + \Psi''(n+1), \tag{A4c}$$

$$
\begin{aligned}
S_l'(n) &= 2^{l-1}\sum_{j=1}^{n}\frac{1+(-1)^j}{j^l}\\
&\to \frac{1}{2}(1+\eta)S_l(n/2)+\frac{1}{2}(1-\eta)S_l((n-1)/2), \quad l=1,2,3,
\end{aligned}
\tag{A4d}
$$

$$
\begin{aligned}
\widetilde{S}(n) &= \sum_{j=1}^{n}\frac{(-1)^j}{j^2}S_1(j)\\
&\to -\frac{5}{8}\zeta(3)+\eta\left\{\frac{S_1(n)}{n^2}-\frac{\zeta(2)}{2}\left[\Psi((n+1)/2)-\Psi(n/2)\right]\right.\\
&\qquad\left.+\int_0^1 dx x^{n-1}\frac{\mathrm{Li}_2(x)}{1+x}\right\},
\end{aligned}
\tag{A4e}
$$

where

$$\gamma_E = 0.577216, \tag{A5a}$$

$$\zeta(2) = \pi^2/6, \tag{A5b}$$

$$\zeta(3) = 1.202057, \tag{A5c}$$

and the Polygamma functions, Ψ, are defined as

$$\Psi^{(m)}(n) = \frac{d^{(m+1)}\Gamma(n)}{dn^{m+1}}. \tag{A6}$$

The integral over the Dilogarithm $\mathrm{Li}_2(x)$ in $\widetilde{S}(n)$ can be calculated analytically by using the approximation:

$$\frac{\mathrm{Li}_2(x)}{1+x} \simeq 0.0030 + 1.0990x - 1.5463x^2 + 3.2860x^3 - 3.7887x^4 + 1.7646x^5, \tag{A7}$$

obtained from a least squares fit. Similar to the fit in Ref. [12], it is a polynomial of degree five, but gives slightly better values for the anomalous dimensions, as can be seen by checking the following relations for the $n = 2$ moments:

$$\gamma_{qq}^{(1),n=2} = -\gamma_{Gq}^{(1),n=2}, \tag{A8a}$$

$$\gamma_{qq}^{(1),n=2} = -\gamma_{Gq}^{(1),n=2}. \tag{A8b}$$

The Polygamma functions must be computed numerically. For the case $|n| > 10$ one applies the asymptotic expansions:

$$\Psi(n) \simeq \ln n - \frac{1}{2n} - \frac{1}{12n^2} + \frac{1}{120n^4} - \frac{1}{256n^6}, \tag{A9a}$$

$$\Psi'(n) \simeq \frac{1}{n} + \frac{1}{2n^2} + \frac{1}{6n^3} - \frac{1}{30n^5} + \frac{1}{42n^7} - \frac{1}{30n^9}, \tag{A9b}$$

$$\Psi''(n) \simeq -\frac{1}{n^2} - \frac{1}{n^3} - \frac{1}{2n^4} + \frac{1}{6n^6} - \frac{1}{6n^8} + \frac{3}{10n^{10}} - \frac{5}{6n^{12}}. \tag{A9c}$$

To obtain greater accuracy for $\Psi''(n)$ we apply an Euler transformation to the asymptotic series in (A9c), ending up with:

$$\Psi''(n) \simeq -\frac{1}{n^2} - \frac{1}{n^3} - \frac{1}{2n^4} + \frac{1}{6n^6} - \frac{1}{16n^8} - \frac{3}{20n^{10}} - \frac{5}{48n^{12}}. \tag{A9d}$$

In the case of $|n| < 10$ the recursion formula

$$\Psi^{(m)}(n+1) = \Psi^{(m)}(n) + (-1)^m m!\; n^{1-m} \tag{A10}$$

is utilized repeatedly [12].

At next-to-leading order, a factor $(-1)^n$ appears in the anomalous dimensions [40] (Eq.(A4)). Therefore the analytic continuation depends on whether the evolution equations for a particular parton distribution are valid for even or odd moments, in which case:

$$(-1)^n \longrightarrow \eta = \pm 1, \tag{A11}$$

for n even or odd, respectively. The η factors relevant for various combinations of parton distributions can be derived from the crossing relations:

$$F_1(-x, Q^2) = +F_1(x, Q^2), \tag{A12a}$$

$$F_{2,3}(-x, Q^2) = -F_{2,3}(x, Q^2). \tag{A12b}$$

For the non-singlet combinations these are (for $N_f = 4$ active flavors) [12]:

$$u - \bar{u} \quad ; \eta = -1 \tag{A13a}$$

$$d - \bar{d} \quad ; \eta = -1 \tag{A13b}$$

$$(u + \bar{u}) - (d + \bar{d}) \quad ; \eta = +1 \tag{A13c}$$

$$(u + \bar{u}) + (d + \bar{d}) - 2(s + \bar{s}) \quad ; \eta = +1 \tag{A13d}$$

$$(u + \bar{u}) + (d + \bar{d}) + s + \bar{s} - 3(c + \bar{c}) \quad ; \eta = +1. \tag{A13e}$$

The singlet distributions are evolved with $\eta = +1$.

2. Polarized DIS

For completeness, we also list the full anomalous dimensions relevant for polarized distributions at NLO. The order α_s anomalous dimensions are given by [2,9]:

$$\gamma_{NS}^{(0),n} = \gamma_{qq}^{(0),n} = 2\,C_F \left[4S_1(n) - 3 - \frac{2}{n(n+1)}\right], \tag{A14a}$$

$$\gamma_{qG}^{(0),n} = 8\,T_F \frac{1-n}{n(n+1)}, \tag{A14b}$$

$$\gamma_{Gq}^{(0),n} = -4\,C_F \frac{n+2}{n(n+1)}, \tag{A14c}$$

$$\gamma_{GG}^{(0),n} = 2\,C_A \left[4S_1(n) - \frac{11}{3} - \frac{8}{n(n+1)}\right] + \frac{8}{3}\,T_F. \tag{A14d}$$

Concerning the order α_s^2, the anomalous dimension $\gamma_{NS,qq}^{(1),n}$ for the non-singlet operator is the same as in the unpolarized case. The singlet dimensions, as evaluated in Ref. [9], are as

follows [2]

$$\gamma_{qq}^{(1),n} = \gamma_{NS,qq}^{(1),n} + \gamma_{PS,qq}^{(1),n}, \tag{A15a}$$

$$\gamma_{PS,qq}^{(1),n} = 16\, C_F T_F \left[\frac{2}{(n+1)^3} + \frac{3}{(n+1)^2} + \frac{1}{(n+1)} + \frac{2}{n^3} - \frac{1}{n^2} - \frac{1}{n}\right], \tag{A15b}$$

$$\begin{aligned}\gamma_{qG}^{(1),n} = 16\, C_A T_F & \left[-\frac{S_1^2(n-1)}{n} + \frac{2\,S_1^2(n-1)}{n+1} - \frac{2\,S_1(n-1)}{n^2} + \frac{4\,S_1(n-1)}{(n+1)^2}\right.\\ & - \frac{S_2(n-1)}{n} + \frac{2\,S_2(n-1)}{n+1} - \frac{2\,\widetilde{S}_2(n-1)}{n} + \frac{4\,\widetilde{S}_2(n-1)}{n+1}\\ & \left. - \frac{4}{n} + \frac{3}{n+1} - \frac{3}{n^2} + \frac{8}{(n+1)^2} + \frac{2}{n^3} + \frac{12}{(n+1)^3}\right]\\ + 8\, C_F T_F & \left[\frac{2\,S_1^2(n-1)}{n} - \frac{4\,S_1^2(n-1)}{n+1} - \frac{2\,S_2(n-1)}{n} + \frac{4\,S_2(n-1)}{n+1}\right.\\ & \left. + \frac{14}{n} - \frac{19}{n+1} - \frac{1}{n^2} - \frac{8}{(n+1)^2} - \frac{2}{n^3} + \frac{4}{(n+1)^3}\right],\end{aligned} \tag{A15c}$$

$$\begin{aligned}\gamma_{Gq}^{(1),n} = 8\, C_A C_F & \left[-\frac{2\,S_1^2(n-1)}{n} + \frac{S_1^2(n-1)}{n+1} + \frac{16\,S_1(n-1)}{3n} - \frac{5S_1(n-1)}{3(n+1)}\right.\\ & + \frac{2S_2(n-1)}{n} - \frac{S_2(n-1)}{n+1} + \frac{4\widetilde{S}_2(n-1)}{n} - \frac{2\widetilde{S}_2(n-1)}{n+1} - \frac{56}{9n}\\ & \left. - \frac{20}{9(n+1)} + \frac{28}{3n^2} - \frac{38}{3(n+1)^2} - \frac{4}{n^3} - \frac{6}{(n+1)^3}\right]\\ + 4\, C_F^2 & \left[\frac{4\,S_1^2(n-1)}{n} - \frac{2\,S_1^2(n-1)}{n+1} - \frac{8\,S_1(n-1)}{n} + \frac{2\,S_1(n-1)}{n+1}\right.\\ & + \frac{8\,S_1(n-1)}{n^2} - \frac{4\,S_1(n-1)}{(n+1)^2} + \frac{4\,S_2(n-1)}{n} - \frac{2\,S_2(n-1)}{n+1}\\ & \left. + \frac{15}{n} - \frac{6}{n+1} - \frac{12}{n^2} + \frac{3}{(n+1)^2} + \frac{4}{n^3} - \frac{2}{(n+1)^3}\right]\\ + 32\, C_F T_F & \left[-\frac{2\,S_1(n-1)}{3\,n} + \frac{S_1(n-1)}{3\,(n+1)} + \frac{7}{9\,n}\right.\\ & \left. - \frac{2}{9\,(n+1)} - \frac{2}{3\,n^2} + \frac{1}{3\,(n+1)^2}\right],\end{aligned} \tag{A15d}$$

[2]Note the correction to the $\gamma_{qG}^{(1),n}, \gamma_{Gq}^{(1),n}$ anomalous dimensions in [9].

$$
\begin{aligned}
\gamma_{GG}^{(1),n} = 4\,C_A^2 \Bigg[& \frac{134}{9}\,S_1(n-1) + \frac{8\,S_1(n-1)}{n^2} - \frac{16\,S_1(n-1)}{(n+1)^2} \\
& + \frac{8\,S_2(n-1)}{n} - \frac{16\,S_2(n-1)}{n+1} + 4\,S_3(n-1) \\
& - 8\,S_{1,2}(n-1) - 8\,S_{2,1}(n-1) + \frac{8\,\widetilde{S}_2(n-1)}{n} - \frac{16\,\widetilde{S}_2(n-1)}{n+1} \\
& + 4\,\widetilde{S}_3(n-1) - 8\,\widetilde{S}_{1,2}(n-1) - \frac{107}{9\,n} + \frac{241}{9\,(n+1)} \\
& + \frac{58}{3\,n^2} - \frac{86}{3\,(n+1)^2} - \frac{8}{n^3} - \frac{48}{(n+1)^3} - \frac{16}{3} \Bigg] \\
+32\,C_A T_F & \left[\frac{-5\,S_1(n-1)}{9} + \frac{14}{9n} - \frac{19}{9\,(n+1)} - \frac{1}{3\,n^2} - \frac{1}{3\,(n+1)^2} + \frac{1}{3} \right] \\
+8\,C_F T_F & \left[-\frac{10}{n+1} + \frac{2}{(n+1)^2} + \frac{4}{(n+1)^3} + 1 + \frac{10}{n} - \frac{10}{n^2} + \frac{4}{n^3} \right].
\end{aligned}
\tag{A15e}
$$

To make use of the anomalous dimensions in the contour evolution method, they must be analytically continued into the complex-n plane. An important fact to observe is that due to the crossing relation:

$$
g_1(-x, Q^2) = -g_1(x, Q^2) \tag{A16}
$$

the OPE relates only *odd* moments of the structure function $g_1(x, Q^2)$ to the sum of possible twist-two operator matrix elements between nucleon states (each multiplied by the appropriate moments of the Wilson coefficient functions). This is contrary to the case of $F_2(x, Q^2)$, where an analogous relation holds for n *even*. To evolve $\Delta\Sigma(x, Q^2)$, $\Delta q_3(x, Q^2)$ and $\Delta q_8(x, Q^2)$ one therefore has to continue the anomalous dimensions from odd n.

In addition to the functions $S_{1,2,3}$, $S'_{1,2,3}$ and $\widetilde{S}$ for the unpolarized anomalous dimensions, for polarized DIS one must also determine the analytic continuation of the functions:

$$
\widetilde{S}_k(n) = \sum_{j=1}^{n} \frac{(-1)^j}{j^k}, \tag{A17}
$$

$$
S_{k,l}(n) = \sum_{j=1}^{n} \frac{S_l(j)}{j^k}, \tag{A18}
$$

$$
\widetilde{S}_{k,l}(n) = \sum_{j=1}^{n} \frac{\widetilde{S}_l(j)}{j^k}. \tag{A19}
$$

Specifically, this must be done for the case of $\widetilde{S}_1$, $\widetilde{S}_2$, $\widetilde{S}_3$, $S_{1,2}$, $S_{2,1}$, and $\widetilde{S}_{1,2}$. Because all

these functions appear with argument $(n-1)$ in Eq.(A15) (see below), one must continue them into complex n starting from even integers n. Using the relation:

$$\sum_{j=1}^{n} \frac{1+(-1)^j}{j^k} = \frac{1}{2^k}\left[(1+\eta)S_k\left(\frac{n}{2}\right) + (1-\eta)S_k\left(\frac{n-1}{2}\right)\right] \tag{A20}$$

with $\eta = +1(-1)$ for n even (odd), a straightforward calculation leads to:

$$\widetilde{S}_k(n) = \frac{1}{2^{k-1}} S_k(n/2) - S_k(n) \tag{A21}$$

for n even. The equality [41]

$$\frac{S_1(j)}{j^2} = \frac{\zeta(2)}{j} - \int_0^1 dx\, x^{j-1} \mathrm{Li}_2(x) \tag{A22}$$

then gives:

$$S_{2,1}(n) = \zeta(2) S_1(n) - \int_0^1 dx\, \frac{x^n - 1}{x-1} \mathrm{Li}_2(x). \tag{A23}$$

The function $S_{1,2}(n)$ can be obtained from the above expressions via [39,41]:

$$S_{1,2}(n) = S_1(n) S_2(n) + S_3(n) - S_{2,1}(n). \tag{A24}$$

The most difficult function to continue is $\widetilde{S}_{1,2}(n)$. For this we start with (see Eq.(A20)):

$$\begin{aligned}\widetilde{S}_{1,2}(n) = &\frac{1}{4}\sum_{j=1}^{n} \frac{S_2(j/2)}{j} + \frac{1}{4}\sum_{j=1}^{n} \frac{(-1)^j S_2(j/2)}{j} \\ &+ \frac{1}{4}\sum_{j=1}^{n} \frac{S_2((j-1)/2)}{j} - \frac{1}{4}\sum_{j=1}^{n} \frac{(-1)^j S_2((j-1)/2)}{j} - \sum_{j=1}^{n} \frac{S_2(j)}{j},\end{aligned} \tag{A25}$$

and apply the relation [41]:

$$S_2(j) = -\frac{S_1(j)}{j} + \zeta(2) + \int_0^1 dx\, x^{j-1} \ln x \;\; \ln(1-x). \tag{A26}$$

After some manipulation one finds:

$$\begin{aligned}\widetilde{S}_{1,2}(n) = &-S_{1,2}(n) + \frac{1}{2}\zeta(2)\left(S_1(n) - \widetilde{S}_1(n)\right) \\ &+ \frac{1}{4}\int_0^1 dx\, \frac{x^{n/2}-1}{x(x-1)} \ln x \ln(1-x) \\ &+ \frac{1}{2}\int_0^1 dx\, \frac{x^{n/2}-1}{x-1} \mathrm{Li}_2(x)\end{aligned}$$

$$+\frac{1}{8}\int_0^1 dx\,\frac{2-2x^{n/2}-nx^{n/2}+nxx^{n/2}}{(x-1)^2}\ln x\ \mathrm{Li}_2(x)$$
$$+\frac{1}{4}\int_0^1 dx\,x^{-3/2}\left(\frac{1}{2}\ln x-1\right)\ln(1-x)\ln\left(\frac{1-\sqrt{x}}{1+\sqrt{x}}\right)$$
$$+\frac{1}{4}\int_0^1 dx\,\frac{x^{n/2-1}}{n+1}\left(\frac{1}{2}\ln x-1\right)\ln(1-x)$$
$$\times\left[{}_2F_1(1,n+1,n+2,\sqrt{x})+{}_2F_1(1,n+1,n+2,-\sqrt{x})\right], \tag{A27}$$

where ${}_2F_1(a,b,c,z)$ is the hypergeometric function. For our application it is convenient to use the integral representation for ${}_2F_1$ [42]:

$${}_2F_1(a,b,c,z)=\frac{\Gamma(c)}{\Gamma(b)\Gamma(c-b)}\int_0^1 dt\,t^{b-1}(1-t)^{c-b-1}(1-tz)^{-a}. \tag{A28}$$

Finally, making the substitution $t\to e^u$ one arrives at:

$${}_2F_1(1,n+1,n+2,z)+{}_2F_1(1,n+1,n+2,-z)=2(n+1)\int_{-\infty}^0 du\frac{e^{(\Re e\,n+1)\,u}}{1-e^{2u}z^2}e^{i(\Im m\,n)\,u}. \tag{A29}$$

APPENDIX B: FACTORIZATION SCHEME DEPENDENCE

In this Appendix we summarize the connection between moments of structure functions and parton distributions in different factorization schemes, which in NLO is not unique. For the moment, $\mathcal{F}_{2,n}^{NS}(Q^2)$, of the non-singlet part of $F_2(x,Q^2)$ we have:

$$\mathcal{F}_{2,n}^{NS}(Q^2)=C_{2,n}^{NS}(Q^2)\ A_n^{NS}(Q^2), \tag{B1}$$

where $C_{2,n}^{NS}(Q^2)$ is the Wilson coefficient, and $A_n^{NS}(Q^2)$ is obtained from the matrix element of the local operator taken between nucleon states. Both quantities on the r.h.s. are factorization scheme dependent. In the $\overline{\mathrm{MS}}$ factorization scheme, for example, the moments of parton distributions are related to $A_n^{NS}(Q^2)$ simply by:

$$\mathcal{Q}_n^{NS}(Q^2)=A_n^{NS}(Q^2). \tag{B2}$$

In the other widely used factorization scheme, namely the DIS scheme, the Wilson coefficient $C_{2,n}^{NS}(Q^2)$ is absorbed into the definition of the moments of parton distributions themselves:

$$C_{2,n}^{NS}(Q^2) \equiv 1. \tag{B3}$$

Therefore $\mathcal{F}_{2,n}^{NS}(Q^2)$ in the DIS scheme is defined to have the same form as in the simple parton model with free quarks.

In analogy, the singlet part of the structure function $F_2(x, Q^2)$ in the DIS scheme must also coincide with the simple parton model result [16]:

$$\mathcal{F}_{2,n}^{S}(Q^2) = \Sigma_n^{\rm DIS}(Q^2). \tag{B4}$$

Here the Wilson coefficient, as well as the gluonic contribution, are absorbed into the singlet quark distribution. However, this procedure does not uniquely fix the gluon distribution. For this one enforces momentum conservation, which leads to the relation [16]:

$$\Sigma_{n=2}^{\rm DIS}(Q^2) + \mathcal{G}_{n=2}^{\rm DIS}(Q^2) = \Sigma_{n=2}^{\overline{\rm MS}}(Q^2) + \mathcal{G}_{n=2}^{\overline{\rm MS}}(Q^2). \tag{B5}$$

To fully define the moments of the gluon distribution one extends this equality to all n.

Since the anomalous dimensions are in a one-to-one correspondence with the renormalization constants of local operators, the evolution equations are affected by transformations to other factorization schemes. Because the renormalization constants depend on the renormalization scheme chosen to renormalize the local operators ($\equiv$ factorization scheme), the anomalous dimensions are factorization scheme dependent. Transforming from the $\overline{\rm MS}$ to the DIS scheme, the anomalous dimensions change according to [43,44]:

$$\boldsymbol{\gamma}_n^{(1),\rm DIS} = \boldsymbol{\gamma}_n^{(1),\overline{\rm MS}} + 2\beta_0 \mathbf{Z}_n^{(1)} - [\boldsymbol{\gamma}_n^{(0)}, \mathbf{Z}_n^1], \tag{B6}$$

$$\mathbf{Z}_n^{(1)} = \begin{cases} C_{2,n}^{(1),q} & \text{nonsinglet}, \\ \begin{pmatrix} C_{2,n}^{(1),q} & C_{2,n}^{(1),G} \\ -C_{2,n}^{(1),q} & -C_{2,n}^{(1),G} \end{pmatrix} & \text{singlet}. \end{cases}$$

From this follow the Q^2 evolution equations in the DIS scheme.

REFERENCES

[1] Yu.L.Dokshitzer, Sov.Phys.-JETP **46** (1977) 641; V.N.Gribov and L.N.Lipatov, Sov.J.Nucl.Phys. **15** (1972) 439, 675; L.N.Lipatov, Sov.J.Nucl.Phys. **20** (1974) 181.

[2] P.Altarelli and G.Parisi, Nucl.Phys. **B126** (1977) 298.

[3] B.Adeva, et al., Phys.Lett. B **329** (1994) 399.

[4] P.L.Anthony, et al., Phys.Rev.Lett. **71** (1993) 959.

[5] R.L.Jaffe and G.G.Ross, Phys.Lett. **B93** (1980) 313.

[6] S.A.Kulagin, W.Melnitchouk, T.Weigl and W.Weise, Nucl.Phys A (1995) in print.

[7] F.E.Close and R.G.Roberts, Phys.Lett. **B316** (1993) 165; J.Ellis and M.Karliner, Phys.Lett. **B313** (1993) 131; G.Altarelli, P.Nason and G.Ridolfi, Phys. Lett. **B320** (1994) 152; P.J.Mulders and S.J.Pollock, Nucl.Phys. **A588** (1995) 876.

[8] A.W.Schreiber, A.W.Thomas and J.T.Londergan, Phys.Lett. **B237** (1990) 120; F.M.Steffens and A.W.Thomas, Adelaide preprint ADP-94-27/T166.

[9] R.Mertig and W.L.van Neerven, preprint NIKHEF-H/95-031 (June 1995); revised (November 1995).

[10] A.D.Martin, R.G.Roberts and W.J.Stirling, Phys.Rev. **D47** (1993) 867.

[11] H.L.Lai, et al., Phys.Rev. **D51** (1995) 4763.

[12] M.Glück, E.Reya and A.Vogt, Z.Phys. **C48** (1990) 471.

[13] S.Kretzer, Phys.Rev. D 52 (1995) 2701.

[14] W.Melnitchouk and A.W.Thomas, Phys.Rev. D 47 (1993) 3794; H.Holtmann, A.Szczurek and J.Speth, Jülich preprint KFA-IKP(TH) 1993-33; E.M.Henley and G.A.Miller, Phys.Lett. B 251 (1990) 497. S.Kumano, Phys.Rev. D 43 (1991) 59, *ibid* 3067; E.Eichten, I.Hinchliffe and C.Quigg, Phys.Rev. D 45 (1993) 2269.

[15] W.Furmanski and R.Petronzio, Z.Phys. **C11** (1982) 293.

[16] G.Altarelli, R.K.Ellis and G.Martinelli, Nucl.Phys. **B143** (1978) 521.

[17] G.Altarelli, Phys.Rep. **C81** (1982) 1.

[18] R.Wilson, Phys.Rev. **179** (1969) 1499.

[19] A.J.Buras, Rev.Mod.Phys. **52** (1980) 199.

[20] R.G.Roberts, *The structure of the proton,* Cambridge University Press, Cambridge (1990).

[21] N.Christ, B.Hasslacher and A.Mueller, Phys.Rev. **D6** (1972) 3543.

[22] T.Muta, *Foundations of quantum chromodynamics,* World Scientific, Singapore (1987).

[23] J.Kodaira, Nucl.Phys. **B165** (1980) 129; E.B.Zijlstra and W.L.van Neerven, Nucl.Phys. **B417** (1994) 61; erratum **B426** 245.

[24] J.Ellis and R.L.Jaffe, Phys.Rev. **D9** (1974) 1444.

[25] M.Miyama and S.Kumano, preprint SAGA-HE-81-95 (1995).

[26] A.W.Schreiber, U. of Adelaide Ph.D. thesis (1991), unpublished.

[27] R.Kobayashi, M.Konuma and S.Kumano, Comput.Phys.Commun. **86** (1995) 264.

[28] G.Fox, Nucl.Phys. **B131** (1977) 107.

[29] IMSL MATH/LIBRARY: User's Manual (Vol.2), Version 1.1 (1989).

[30] K.S.Crump, J.Assoc.Comput.Mach. **23** (1976) 89.

[31] J.G.Morfin and W.-K.Tung, Z.Phys. **C52** (1991) 13.

[32] M.Aguilar-Benitez, et al., Phys.Rev. **D50** (1994) 1173.

[33] M.Glück, E.Reya, M.Stratmann and W.Vogelsang, Dortmund preprint DO-TH 95/13

(1995).

[34] R.D.Ball, S.Forte and G.Ridolfi, preprint CERN-TH/95-266 (1995).

[35] W.Vogelsang, preprint RAL-TR-95-071 (1995).

[36] T.Gehrmann and W.J.Stirling, Z.Phys. **C65** (1995) 461.

[37] R.Hamberg and W.L.van Neerven Nucl.Phys. **B359** (1991) 343.

[38] E.G.Floratos, C.Kounnas and R.Lacaze, Nucl.Phys. **B192** (1981) 417.

[39] A.Gonzales-Arroyo, C.Lopez and F.J.Yndurain, Nucl.Phys **B153** (1979) 161.

[40] D.A.Ross and C.T.Sachrajda, Nucl.Phys. **B149** (1979) 497.

[41] A.Devoto and D.W.Duke, Riv.Nuov.Cim. **7-6** (1984) 1.

[42] M.Abramowitz and I.A.Stegun, *Handbook of mathematical functions,* Dover, New York (1968).

[43] M.Diemoz, et al. Z.Phys. **C39** (1988) 21.

[44] M.Glück, and E.Reya, Phys.Rev. **D25** (1982) 1211.

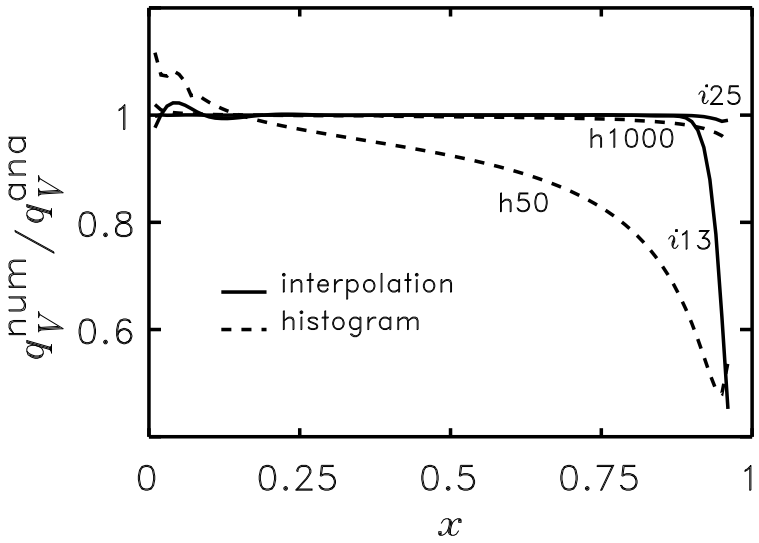

FIG. 1. Ratio of evolution results for $q_V = u_V + d_V$ obtained by calculating moments numerically ($q_V^{\rm num}$) and analytically ($q_V^{\rm ana}$). For comparison, two methods for calculating the moments numerically (interpolation and histogram) have been applied, using various numbers of points in Bjorken-x (given on top of the lines accompanied by a letter indicating the method used).

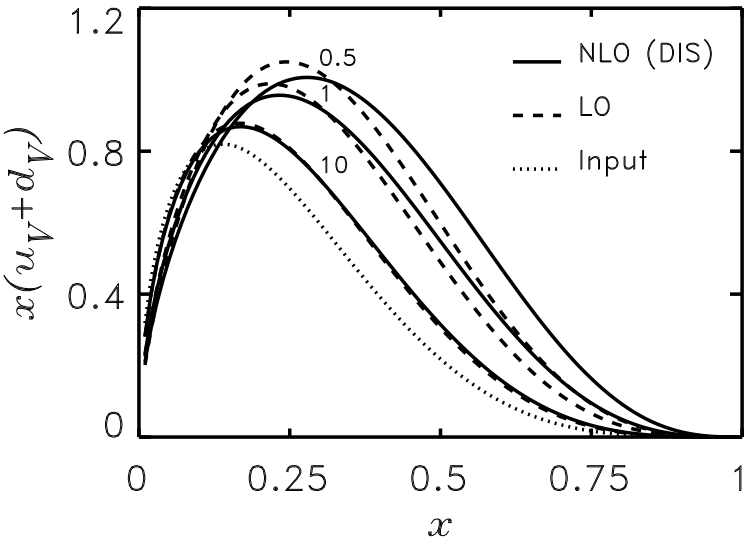

FIG. 2. Comparison of LO and NLO (DIS-scheme) evolution of the total valence distribution $x(u_V + d_V)$. Input taken from the latest CTEQ fit [11] is evolved from $Q^2 = 100$ GeV^2 down to different values of Q^2 (given on top of the corresponding lines).

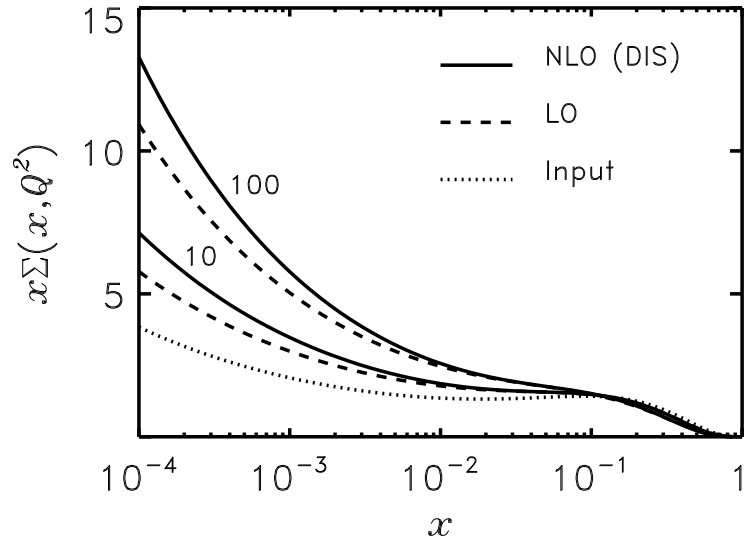

FIG. 3. Comparison of LO and NLO (DIS scheme) evolution of the singlet distribution $x\Sigma(x, Q^2)$. Values of Q^2 are attached to corresponding pairs of lines.

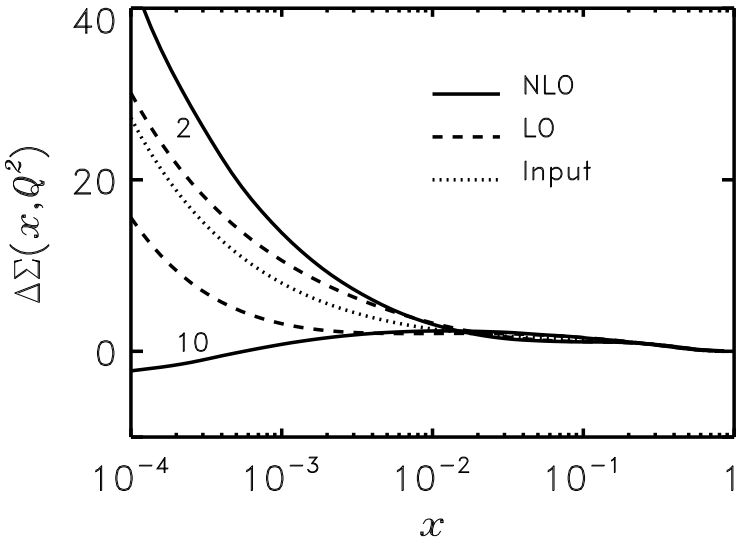

FIG. 4. Comparison of LO and NLO evolution of the polarized singlet distribution $x\Delta\Sigma(x,Q^2)$. Input is taken from Ref. [36] (Set A). Values of Q^2 are given for each pair of lines.

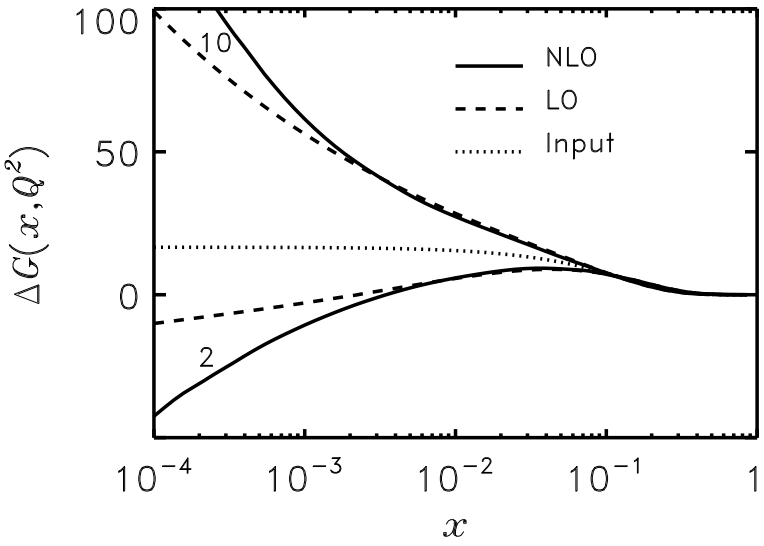

FIG. 5. Comparison of LO and NLO evolution of the polarized gluon distribution $x\Delta G(x,Q^2)$. Values of Q^2 are attached to corresponding pairs of lines.

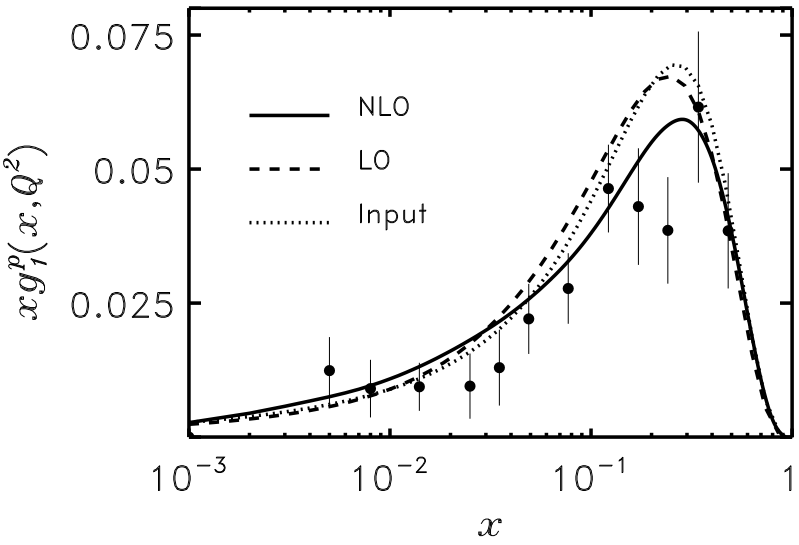

FIG. 6. NLO effects on the shape of the structure function g_1^p. Data shown are from the SMC [3] at an averaged value of $\langle Q^2 \rangle = 10$ GeV^2, to which also the input has been evolved.

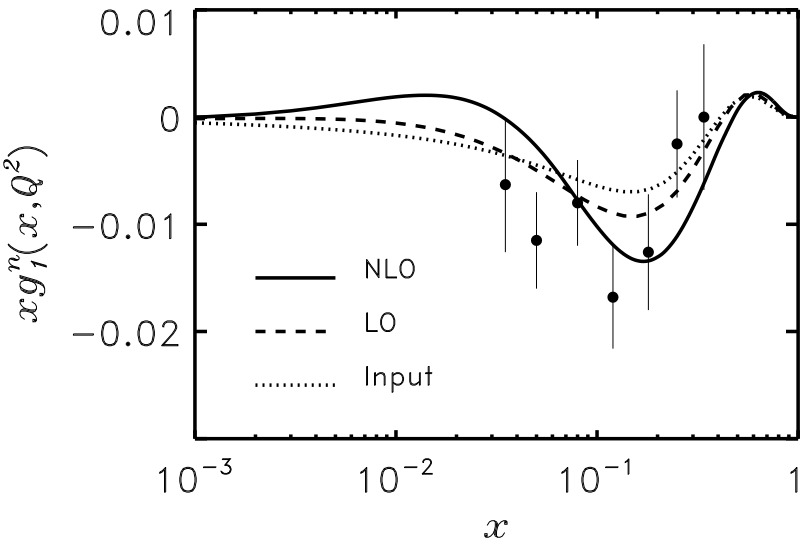

FIG. 7. NLO effects on the shape of the structure function g_1^n. Input is evolved to 2 GeV^2 for comparison with the SLAC E142 data [4].